Aridity events during the last 4000 years in Western Mediterranean marshes (Almenara and Benicasim marshes, E Spain)

J.F. Mediato, J.I. Santisteban, B. del Moral, R. Mediavilla, C.J. Dabrio

PII: S1040-6182(20)30185-3

DOI: https://doi.org/10.1016/j.quaint.2020.04.021

Reference: JQI 8247

To appear in: *Quaternary International*

Received Date: 14 February 2020

Revised Date: 11 April 2020

Accepted Date: 15 April 2020

Please cite this article as: Mediato, J.F., Santisteban, J.I., del Moral, B., Mediavilla, R., Dabrio, C.J., Aridity events during the last 4000 years in Western Mediterranean marshes (Almenara and Benicasim marshes, E Spain), *Quaternary International* (2020), doi: https://doi.org/10.1016/j.quaint.2020.04.021.

Aridity events during the last 4000 years in Western Mediterranean marshes (Almenara and Benicasim marshes, E Spain).

J.F. Mediato [a], J.I. Santisteban [b], B. del Moral [c], R. Mediavilla [a], C.J. Dabrio.[b]

a Departament of Geological Resources Research, Geological Survey of Spain (IGME), C/Rios Rosas 23, 28003-Madrid, Spain

b Departament of Geodynamics, Stratigraphy and Paleontology, Complutense University of Madrid, C/José Antonio Novais 12, 28040-Madrid, Spain

c Departament of Geoscientific Infrastructure and Services (Laboratory), Geological Survey of Spain (IGME), C/Calera 1, 28760-Tres Cantos, Madrid, Spain

Abstract

Facies and geochemical analysis applied marsh deposits are useful proxies for the reconstruction of aridity for the last millennia. The comparison of facies and geochemical records among cores from the Almenara and Benicasim marshes allows to identify changes in water level (Si/Al, Al, Ca) and salinity of the feeding waters (Mg/Al, Na/Al, S/Al). These changes, in turn, represent fluctuations in the position of the saline-fresh groundwater boundary, which can be related to variations in sea level and rainfall. For the last 4000 years, three events recording higher salinity conditions (ca. 3.8 ka BP, ca. 3 ka BP and ca. 1.8 ka BP) are noticeable in the record. Comparison to other studies around the Western Mediterranean basin allows us to correlate these events to arid periods and to identify their forcing mechanisms. These aridity events are correlative to small falls in solar activity and Surface Sea Temperature (SST) during positive North Atlantic Oscillation (NAO) periods. Despite the small magnitude of these changes, the sensitivity of the system amplified the result providing a conspicuous signal.

Keywords: Mediterranean coastal marshes, geochemical and facies proxies, aridity periods, sea level, Holocene.

1. Introduction

The Iberian Peninsula is located between the Eurosiberian, which is characterized by a cold and humid climate without seasonality, and the Mediterranean, with droughts in summer and relatively cold and humid winters, regions (Giralt et al., 2017). This climatic setting and the relief of the Iberian Peninsula give place to a multitude of micro-climates with different temporal and spatial sensitivities. Consequently, to achieve a good knowledge of the climate of the Western Mediterranean basin, a detailed characterization in space and time is needed.

Paleoclimatic reconstructions from lakes for the last 4000 years with, at least, millennial resolution are located mainly in the northern and southern areas of Spain: Arreo Lake (Corella et al., 2013), Estanya Lake (Morellón et al., 2011), Siles Lake (Carrión, 2002), Zoñar Lake (Martín-Puertas et al., 2008), Padul Lake (Ramos-Román et al., 2018) and are scarce in central Spain. The lacustrine records studied in the central Spain are rare: i.e. Las Tablas de Daimiel (Mediavilla et al., 2013; Santisteban et al., 2019) giving an incomplete picture of the climatic evolution for this period (Giralt et al., 2017).

In this paper, we study two coastal marshes in the central Mediterranean coast of Spain in order to disentangle the influence of sea level and climate on their evolution. To achieve this goal, facies and geochemical proxies are used to reconstruct their paleohydrological changes and, later, to link these to identify their forcings via the correlation with other regional records.

Coastal wetlands in E Spain were formed by the migration of coastal barriers upon old Pleistocene alluvial deposits during the Holocene highstand that resulted in the closure of bays and lagoons around mid-Holocene times. They are typical features of the coastal plain landscapes of the Spanish Mediterranean coast: Mar Menor, Valencia lagoon, Oliva-Pego marsh, Almenara, Benicasim and Torreblanca-Cabanes marshes. Previous sedimentological, geomorphological and paleontological studies focused on their paleoenvironmental reconstruction during the Holocene (Dupré et al., 1988; Usera et al., 1996, 2002; Mediato and Santisteban, 2006; Carmona and Ruiz, 2011; Marco-Barba et al., 2013, Carmona et al., 2016; Mediato, 2016; Blázquez et al., 2017, 2018; Rodríguez-Pérez et al., 2018; Ruiz-Pérez and Carmona, 2019; López-Belzunce et al., 2020). These studies concluded that the Holocene paleoenvironmental changes were related to the eustatic variations that took place since the Last Glacial Maximum and climate was a minor forcing of local interest. After the stabilization of the sea level at the Holocene highstand, only minor variations were recorded and mostly linked to local factors (Goy et al., 2003; Mediato and Santisteban, 2006). For most of the last 4000 years, coastal wetlands have no direct connection to the sea. In the case of the marshes of Almenara and Benicasim, the paleoecological studies (foraminifers and ostracods) show that they were oligohaline marshes only affected by small fluctuations in their water levels (Usera et al., 1996; Mediato, 2016; Blázquez et al., 2017, 2018; Rodríguez-Pérez et al., 2018). These authors did not reach conclusive paleoecological data that allowed distinguishing relative changes in salinity of wetlands during the period.

2. Regional setting

The study area is located in the central sector of the Spanish Mediterranean coast (Fig. 1) and it is characterized by a narrow coastal plain composed by coastal deposits (beaches and marshes) bounded by gently seawards dipping alluvial plains linked to the nearby mountain front.

Climate is typical of a semi-arid Mediterranean area. The interannual thermal regime is quite regular (Martin-Vide, 1997), being the distribution of the Mediterranean basin itself, with moderately cold winters, around 11ºC (January), and hot summers, with an average of 25ºC (August) and annual averages around 17ºC. Average annual rainfall is around 450 mm (Montón and Quereda, 1997) with rainy autumns and dry summers. Annual evapotranspiration potential ranges from 750 and 800 mm, and estimated actual evapotranspiration is 450-500 mm, resulting in very dry conditions.

Present day configuration originated during the opening of the Valencia Through at Upper Oligocene - Lower Miocene times (Fontboté et al., 1990; Roca et al., 2001; Vegas and Vicente, 2004). It is bounded by NE-SO and E–O faults with Mesozoic rocks forming the uplifted blocks (Simón, 1984), to the West, and opened to the Mediterranean Sea, to the East.

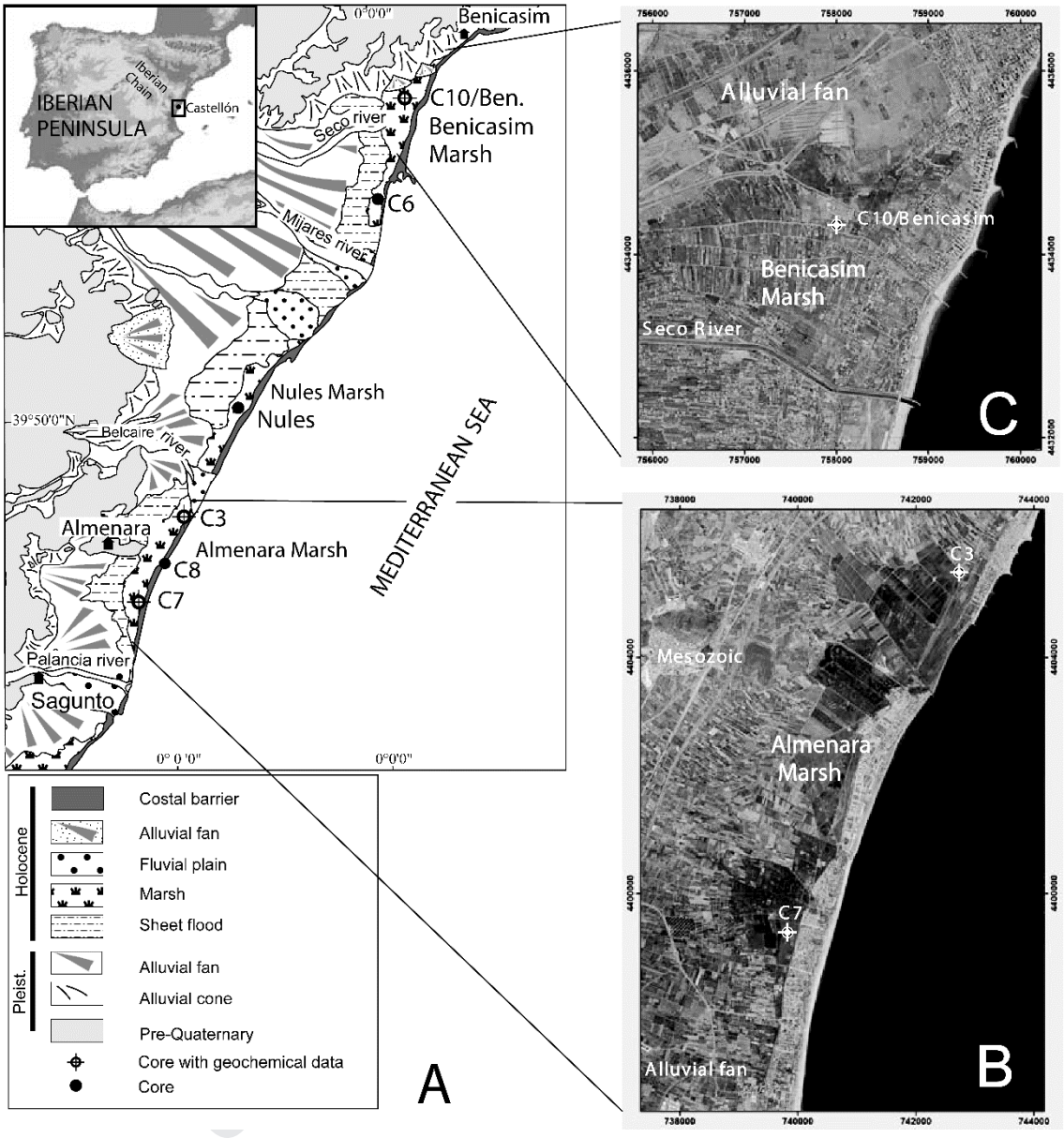

Figure 1. *(a) Geographical and geological setting and location of cores. Detail of Almenara (b) and (c) Benicasim mashes and position of the cores with geochemical data. Orthophotos provided by the Spanish Geographical Institute (IGN).*

This depression is filled by Neogene and Quaternary clastic sediments (Goy, 1978; Simón, 1984). Quaternary is mainly composed by Upper Pleistocene alluvial fan deposits (Mediato et al., 2015).

Just after the Holocene sea level maximum, the coast was composed by open bays placed between river mouths/deltas and/or Mesozoic tectonic reliefs. The longshore transport towards the S of the sediments supplied by the rivers allowed the formation of spit bars that progressively closed those bays, giving place to the development of the present day marshes (Mediato, 2016).

Thus, the Holocene record is composed by terrestrial (alluvial fan, sheetflood and fluvial) and coastal (beaches, bay, freshwater marsh and lagoon) deposits (Mediato and Santisteban, 2006; Mediato, 2016) (Fig. 1).

The Almenara marsh is bounded by the Palancia and Belcaire rivers, upon whose fluvial deposits it rests. The Belcaire river (to the N) supplied the clastic sediments that formed the coastal barrier that closed a previous open bay (Mediato and Santisteban, 2006). Nowadays, the area is composed by several small lakes covering a surface of about 1200x1000 m, with depths up to ten meters, and its hydrology is man-controlled. It is the only wetland in the area that still preserves some areas with natural flora and fauna with *Lemnetea*, *Potametea* and *Charophyte* elements in the open, clear water areas and *Typho - Scirpetum tabernaemontani* (*Phragmites australis*, *Scirpus lacustris* and *Typha latifolia* and *angustifolia*) or *Typha angustifoliae - Phragmitetum maximi* (*Phragmites maximus, Typha angustifolia, Epilobium hirsutum, Lycopus europaeus* and *Kosteletzkya pentacarpos*) associations in the borders (Fullana, 2001). The outermost belt is made up of dense grasslands and small-sized rushes (*Magnocaricion*) that do not get flooded (Viñals and Fumanal, 1995).

The Benicasim marsh is placed between Mesozoic reliefs (to the North and West) and the Pleistocene alluvial fan of the Mijares river (to the South). The marsh is crossed by the Seco river, a currently channelled ephemeral river. Nowadays, the marsh is inactive due to man action but, until the 1950s, it was used for rice pads and peat extraction.

Both marshes are linked to the outcrop of the groundwaters of a Plio-Pleistocene siliciclastic aquifer that is characterized by Cl^-, Na^+ and K^+ (Tuñón, 2000) and SO_4^+ content related to sea water intrusion. It is consequence of a decrease in natural flow of freshwater due to artificial extractions.

In natural conditions the water level of the wetlands is controlled by the hydraulic gradients between terrestrial freshwaters (surface and groundwaters) and the marine saline waters which, in turn, depend on the sea level (the ultimate base level) and the freshwater discharge. Thus, sea level and water budget changes are the main controls on the wetland evolution.

3. Material and methods

Four cores were recovered in the Almenara-Nules marshes and two in the Benicasim marsh. (Fig. 1). Detailed stratigraphic sections were corrected for depth (to account for compaction during the drilling). Each core was described: lithology, grain size, colour, texture, fossil content and sedimentary structures and facies sequences were defined (Fig. 2). The uppermost two cycles of three of such cores (C3, C7 and C10) were sampled for geochemistry and mineralogy as these cycles can be correlated among cores (Fig. 2).

Mineralogy was analysed at the Spanish Geological Survey by XRD. Bulk sample and the <2 μm fraction were used for mineral identification. 23 samples were taken in selected positions for facies characterization.

Geochemical analyses were carried out in the laboratories of ALS Chemex in Canada. Si, Al, Fe, Ca, Mg, Na, K, Cr, Ti, Mn, P, Sr, Ba oxides and B and S were determined by X-ray Fluorescence (XRF) and Infrared Spectrometry (IR). Inorganic C and organic C were determined by coulometry and IR. 10 mm-thick samples were taken contiguous resulting in 413 samples.

Principal Component Analysis was carried out on the geochemical data in order to analyse the relations among elements and relate such compositions to mineralogy and lithofacies.

14 AMS ^{14}C and standard ^{14}C samples (vegetal remains and organic matter) for the six cores were dated at the GADAM Centre (Gliwice, Poland). Dates were calibrated with CALIB 7.1 (Stuiver and Reimer, 1986, 1993; Stuiver et al., 2015), using the IntCal 13 curve (Reimer et al., 2013) (Table 1).

Core	Lab Sample number	Depth (cm)	^{14}C age (BP)	Method	$\delta^{13}C$	Lithology	Calibrated ^{14}C age (2σ)
C 3	GdA-657	21	715 ± 35	AMS	-10,8 ± 0,4	Silt	[644-724 BP]
C 3	GdA-658	51	820 ± 35	AMS	-22,6 ± 0,7	Silt	[679-789 BP]
C 3	Gd-30095	157	4870 ± 100	Radiocarbon standard	-25	Peat	[5445-5766 BP]
C 6	GdA-649	79	610 ± 35	AMS	-31,5 ± 0,6	Peat	[544-656 BP]
C 6	GdA-648	265	3690 ± 35	AMS	25,6 ± 0,5		[3922-4098 BP]
C 7	GdA-650	130	Modern 114,96 ± 0,41 pMC	AMS	-25,9 ± 0,2	Organic-rich sediment	-----
C 7	Gd-30096	344	5020 ± 120	Radiocarbon standard	-25	Peat	[5576-6003 BP]
C 8	GdA-651	69	Modern 124,43 ± 0,46 pMC	AMS	-28,6 ± 0,3	Organic-rich sediment	-----
C 8	Gd-17366	172	3800 ± 140	Radiocarbon standard	-25	Peat	[3826-4574 BP]
C 10	GdA-616	48	Modern 109,68±0,37 pMC	AMS	-30,7 ± 0,6	Organic-rich sediment	-----
C 10	GdA-501	140	270 ± 40	AMS	-28,8 ± 0,4	Peat	[346-464 BP]
C 10	Gd-30094	191	3320 ± 95	Radiocarbon standard	-25	Peat	[3366-3732 BP]
Benicasim	GdA-500	360	5150 ± 40	AMS	-26,3 ± 0,9	Peat	[5875-5991 BP]
Nules	GdA-503	485	5920 ± 70	AMS	-29,3 ± 0,3	Peat	[6601-6936 BP]

Table 1. *Radiocarbon samples and dates for the studied cores.*

4. Results

4.1. Facies, environments and sequences.

Facies description and interpretation is based on cores observation and present environments distribution. Five facies have been identified for the studied sections: four marsh facies and one alluvial facies present at the top of the cores (Fig. 2). In addition, sandy facies interpreted as back-barrier/washover fan deposits (Mediato, 2016) are commonly found below these facies.

Marsh facies are:

a) Green to grey clays (external marsh facies). Massive clay levels (3 to 25 cm in thickness) composed by illite, chlorite, small amounts of calcite and quartz, gypsum is common. They contain vegetal remains and well-preserved gastropoda shells (*Hydrobia* sp, *Planorbis* sp. and *Bithynia* sp.). Calcite is found as sparse millimetre-size nodules or cementing root traces. They are interpreted as deposited in the external areas of the marsh, where external clastic inputs were waterlogged, colonized by vegetation and occasionally exposed.
b) Peat (intermediate marsh facies). Brown to black sapric and hemic peat levels (1 to 60 cm in thickness) with variable amounts of quartz, phyllosilicates, microcline, calcite and, rarely, gypsum. Well-preserved ostracoda, gastropoda and foraminifera shells are common. The most frequent foraminifera are *Ammonia tepida* (Cushman), *Trichohyalus aguayoi* (Bermúdez) and *Trochammina inflata* (Montagu). *Cyprideis torosa* (Jones) is

the most abundant ostracoda. They represent the vegetated fringe located between the external areas of the marsh and the semi-permanent open water areas.

c) Carbonated muds (intermediate marsh facies). Massive levels (7 to 30 cm in thickness) of grey muds composed by calcite with small amounts of quartz, muscovite and organic matter. They contain charophycea remains (stems and oogonia), ostracoda, benthic foraminifera and gastropoda shells (*Bithynia* sp., *Limnaea* sp. *and Planorbis* sp.). The most frequent foraminifera are *Ammonia tepida* (Cushman) and *Trichohyalus aguayoi* (Bermúdez). *Cyprideis torosa* (Jones) is the most abundant ostracoda. They are interpreted as intermediate water depth marsh areas, located between the peat forming areas and the inner marsh, were clastic inputs can still arrive.

d) Biogenic carbonates (inner marsh facies). White to cream calcitic levels (2 to 5 cm in thickness). They are mostly composed by charophyte remains (stems and oogonia) with some ostracoda, benthic foraminifera and gastropoda shells (*Bithynia* sp, *Limnaea* sp. and *Hydrobia* sp) immersed in a micritic matrix. Laminations produced by waves can be recognized. It is composed only of calcite. These deposits are interpreted as the accumulation of charophytes in the inner open water areas of the marsh.

Alluvial facies are composed by pale brown massive or laminated siliciclastic muds and silts with variable amounts of clay and fossil remains (fragments of gastropods and plants). Root traces are common. Their mineralogy is composed by clay (illite and kaolinite) and quartz. They also contain calcite and/or dolomite nodules and lenticular gypsum in relation to root traces. The lower boundary of the beds can be an erosive surface paved with small clasts. To the top, the beds is usually gleyed and carbonate nodules are present. They are interpreted as distal alluvial fan or sheet flood facies.

These facies arrange in (Fig. 2):

a) Deepening-upwards sequences composed by external marsh or peat facies followed by carbonated mud and inner marsh facies. No alluvial facies have been observed at the base of these sequences.

b) Shallowing-upwards sequences composed by inner or intermediate facies (peat or carbonated mud) followed by peat, external of alluvial facies. No carbonated mud or inner marsh facies are recorded at the top of these sequences.

These sequences form deepening-shallowing cycles with a usually thinner lower deepening sequence and a thicker upper shallowing one. It is not uncommon that, being the lower (deepening) sequence too thin, the cycle seems to be represented only by the shallowing-upwards term.

These cycles can be correlated among cores providing, in addition to the radiocarbon dates, an approximate chronological framework (Fig. 2). The uppermost two cycles show the complete set of marsh facies and they can be considered continuous in time as there are no erosive surfaces (unless for some minor ones in the alluvial facies) and the recorded facies reveal the spatial continuity of recorded environments (Walther's Law; Walther, 1894). Thus, these cycles are the most suitable for a study in detail.

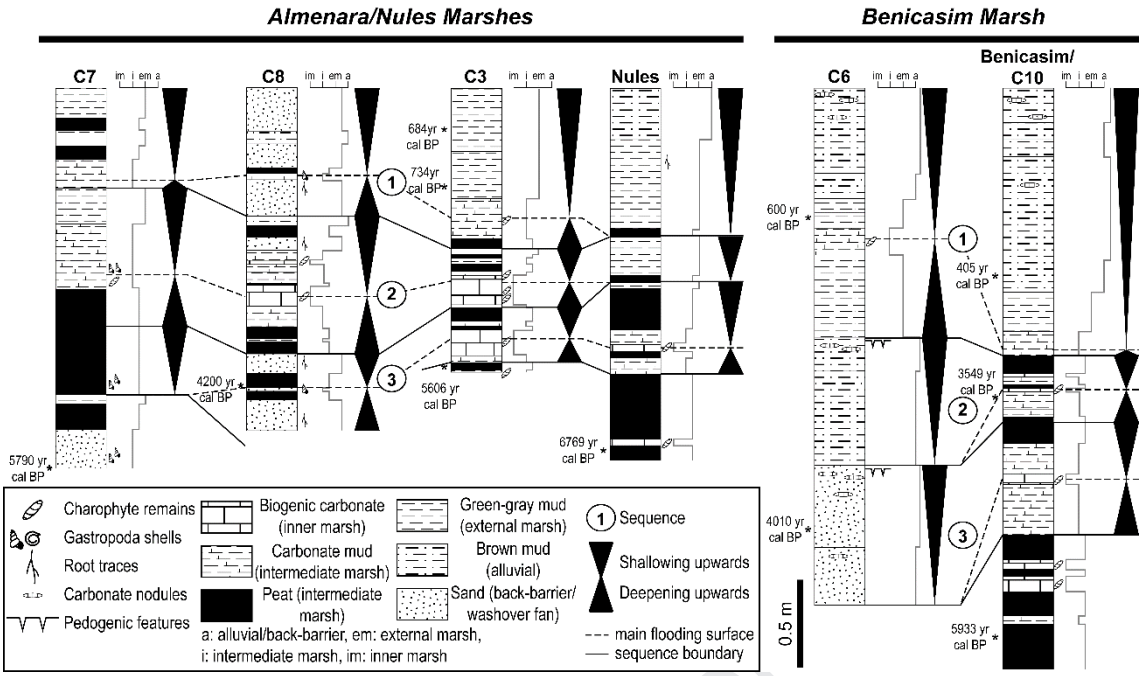

Figure 2. *Stratigraphic sections for cores recovered at Almenara-Nules and Benicasim marshes with indication of facies, environments and sequences/cycles (modified from Mediato, 2016).*

4.2 Geochemical proxies

A Principal Component Analysis (PCA) has been carried on the geochemical data from the cores to explore the relations among geochemical elements and their environmental interpretation (Fig. 3, Table 2). The analysis reveals that the first two principal components (PC1 and PC2) explain most of the variance of the geochemical data (84% for C3, 78% for C7 and 74% for C10).

PC1 shows the reverse relation between the carbonated (Ca, inorganic C and Sr), internal sediment production, and siliciclastic components (Si, Al, Fe, Mg, Na, K, etc.), external sediment inputs. On the other hand, PC2 points to a relation between organic components (organic C, S, P), linked to reducing conditions, and chemically precipitated elements (Ca, Sr, Na, Mg, Mn) related to bioprecipitation of carbonate (Charophytes) and oxygenated bottom waters. Thus, these PCs are related to the main lithofacies present in the marshes (siliciclastics, carbonates and peat).

In order to analyse other relations, and after checking that the mineralogical composition showed no major changes in the silicate fraction, the values were normalized against Al (with an exclusive siliciclastic origin) to check if the departures of siliciclastic-related elements could be linked to other origins (Calvert and Pedersen, 2007). Another time, most of the variance is explained by the two main PCs for the Al-normalized values (79 % for C3, 76 % for C7 and 70% for C10).

The main PC shows a reverse relation among clay-related components (K/Al and Ti/Al) and organic-saline-redox components (i.e. Ca/Al, Sr/Al, Na/Al, Mg/Al, S/Al, organic and inorganic C/Al, P/Al, Fe/Al, Mn/Al). PC2 strengthens this idea as illustrates the reverse relation among siliciclastic (i.e. Si/Al, Ti/Al) and saline (i.e. Na/Al, Sr/Al) components.

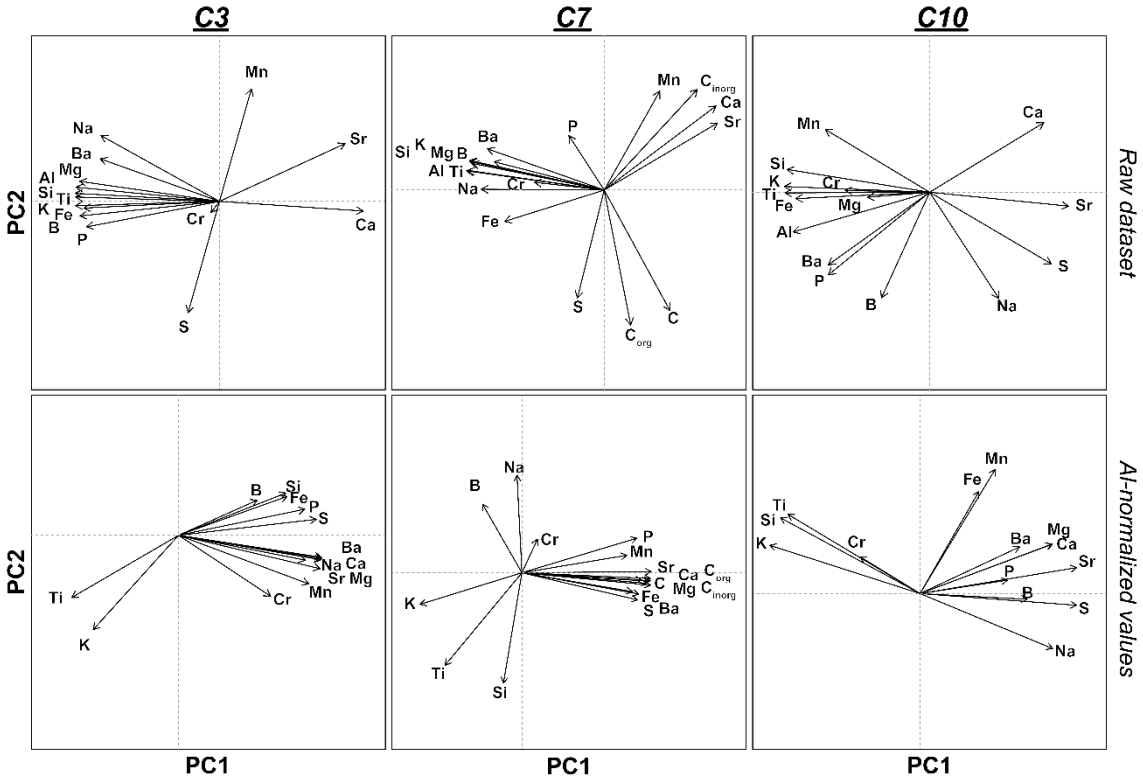

229

230 ***Figure 3.*** *Biplot of the two main principal components for the raw geochemical dataset and*
231 *the Al-normalized values.*

	Raw dataset						Al-normalized values						
	C7		**C3**		**C10**			**C7**		**C3**		**C10**	
	PC1	PC2	PC1	PC2	PC1	PC2		PC1	PC2	PC1	PC2	PC1	PC2
Al	**-0.303**	0.059	**-0.290**	0.074	***0.295***	-0.164							
Si	**-0.296**	0.091	**-0.291**	0.043	***0.308***	0.094	Si/Al	-0.040	**-0.547**	***0.184***	***0.363***	***0.292***	***0.330***
Fe	**-0.219**	-0.096	**-0.274**	-0.035	***0.290***	-0.027	Fe/Al	***0.241***	-0.094	***0.231***	-0.095	-0.123	***0.445***
Ca	***0.246***	***0.258***	***0.290***	-0.051	**-0.247**	***0.288***	Ca/Al	***0.281***	-0.040	***0.251***	-0.002	**-0.277**	***0.215***
Mg	**-0.297**	0.088	**-0.283**	***0.105***	0.135	-0.021	Mg/Al	***0.281***	-0.061	***0.248***	0.034	**-0.276**	***0.215***
Na	**-0.270**	0.002	**-0.240**	***0.346***	-0.150	**-0.440**	Na/Al	-0.011	***0.483***	***0.216***	***0.318***	**-0.277**	**-0.240**
K	**-0.291**	0.082	**-0.291**	-0.023	***0.315***	0.024	K/Al	**-0.222**	-0.156	**-0.170**	***-0.491***	***0.314***	***0.210***
Cr	-0.153	0.024	-0.017	-0.058	0.183	0.007	Cr/Al	0.034	0.167	***0.178***	-0.216	0.125	***0.160***
Ti	**-0.300**	0.061	**-0.291**	0.023	***0.313***	-0.003	Ti/Al	**-0.168**	**-0.459**	**-0.182**	***-0.500***	***0.276***	***0.345***
Mn	0.122	***0.303***	0.065	***0.590***	***0.226***	***0.260***	Mn/Al	***0.229***	0.086	***0.223***	-0.149	-0.157	***0.540***
P	-0.078	0.167	**-0.268**	-0.133	***0.219***	**-0.342**	P/Al	***0.251***	0.171	***0.246***	-0.065	-0.183	0.058
Sr	***0.250***	***0.206***	***0.254***	***0.303***	**-0.300**	-0.058	Sr/Al	***0.282***	0.006	***0.247***	-0.025	**-0.328**	***0.113***
Ba	**-0.257**	0.127	**-0.241**	0.223	***0.219***	**-0.301**	Ba/Al	***0.255***	-0.105	***0.250***	-0.024	**-0.208**	***0.203***
B	**-0.242**	0.087	**-0.282**	-0.076	0.104	**-0.437**	B/Al	-0.086	***0.340***	***0.201***	***-0.376***	**-0.224**	-0.025
S	-0.059	**-0.331**	-0.063	**-0.584**	**-0.263**	**-0.296**	S/Al	***0.253***	-0.135	***0.251***	-0.138	**-0.327**	-0.051
C_{in}	***0.205***	***0.309***					C_{in}/Al	***0.273***	-0.052				
C_{org}	0.058	**-0.414**					C_{org}/Al	***0.261***	-0.036				

232 ***Table 2.*** *Eigenvectors for the two main principal components for the raw geochemical*
233 *dataset and the Al-normalized values. Bold-italics: main positive values; bold: main*
234 *negative values.*

235 From the information provided by the PCA, a set of environmental proxies were chosen:

236 a) external siliciclastic inputs (Al, Si/Al indicative of the quartz/clay or grains/matrix ratio,
237 Santisteban et al., 2019),
238 b) carbonate precipitation (Ca, inorganic C),

c) salinity proxies linked to marine waters (Mg/Al, Na/Al, Sr/Al, S/Al) (Giménez, 1994; Morrell et al, 1996; Giménez and Morell, 1997; Tuñón, 2000) or terrestrial origin (S/Al, that can be also related to organic matter content),
d) redox conditions (Mn/Fe, Egstrom y Hansen; 1985; Mackereth, 1966) which shows its higher values for carbonate bearing beds (Charophyte layers) and decreases for peat layers indicating reducing conditions.

The geochemical record for cycles 1 and 2 shows the following features (Fig. 4):

1) All of them show an overall shallowing upwards trend from intermediate-internal marsh facies to alluvial facies that it is recorded in the increase in Al.
2) As pointed by PCA, siliciclastics (Si/Al, Al) are opposed to carbonates (Ca, inorganic C). Calcite is part of the structure of the Charophyte that need clean and well-oxygenated waters. So, Ca is related to high lake level phases and high Mn/Fe ratios. Increases in the Si/Al ratio can be interpreted as increases in quartz/clay minerals ratio which, in turn, represent changes in grains/matrix ratio (Santisteban et al., 2019). The quartz source can be placed both in the beach-barrier (clay-poor inputs related to storms) or in inland areas (from surface runoff during floods and/or during low water levels, usually together with clay minerals).
3) Peats layers, formed at the margin of the marsh, commonly show high Al values, that record the trapping of the clay by the vegetation, and low Mn/Fe ratios, recording the reducing conditions linked to the accumulation of organic matter.
4) Mg/Al and S/Al use to be correlated to Ca. As there are no saline minerals in the inner and intermediate marsh facies, these elements must be present in the clay fraction, organic matter or, for Mg, substituting Ca in calcite. Mg and S can be related to changes in salinity linked to marine waters, richer in such elements.
5) Na/Al shows a complex behaviour as its values, in average, use to be high as the other saline elements but, in detail, Na shows changes that can be both directly and reversely correlated to them.

About the changes in time and space of geochemical proxies, all the selected geochemical proxies show a similar behaviour in C3 and C10, with higher values of Ca, Mg/Al, S/Al and Na/Al and lower values of Al for cycle 2, and increase in Al and decrease in Ca, Mg/Al, S/Al and Na/Al for cycle 1. C7 shows similar minor oscillations than the other cores but there are no evident overall trends in the cycles.

It is noticeable the presence of three peaks in the salinity proxies that can be placed in the three cores. They are placed in relation to the higher water levels of cycles 1 and 2 (changing point from deepening to shallowing trend) and in a carbonate (high water) level in the upper sequence of cycle 2. There are no common peaks of salinity proxies for the shallowing upwards sequence of cycle 1.

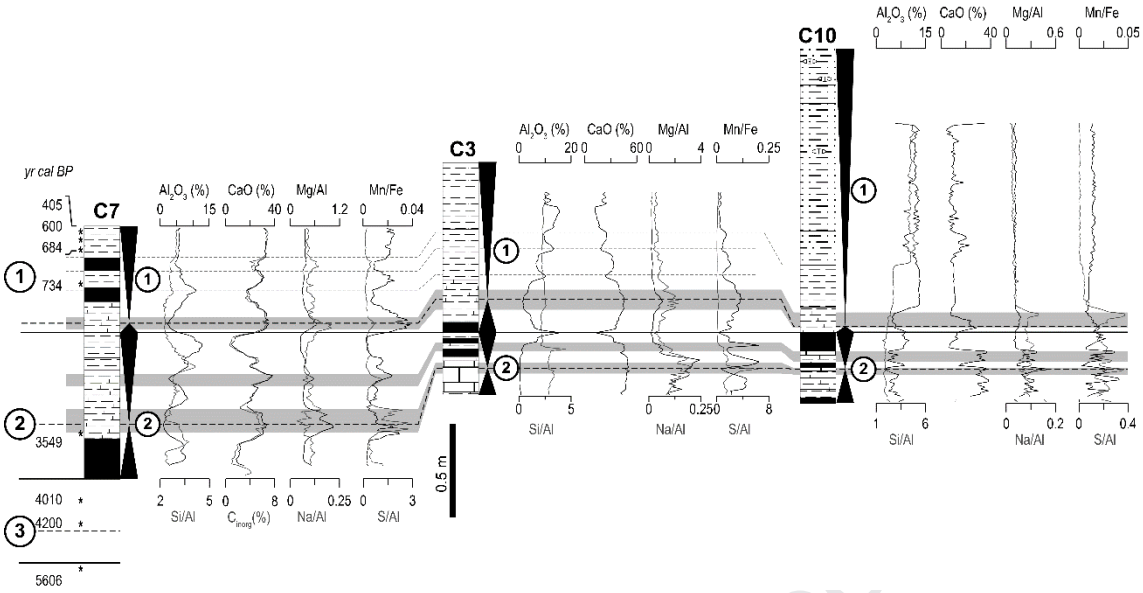

Figure 4. *Facies and geochemical record for the cored of Almenara and Benicasim marshes for cycles 1 and 2. Facies and trend key as for figure 2. Radiocarbon samples (from the whole set of cores in Fig. 2) arrangement relative to sequence boundaries. Grey stripes: Ca, Mg/Al, S/Al, Na/Al and Mn/Fe increases.*

5. Discussion

As mentioned in the introduction, the key for understanding and interpreting these environments is the fact that the level and quality of the waters of the marsh and the stratigraphic architecture of these systems are ruled by:

1) The water budget.
2) The base level, which for these marshes is determined by the sea level.
3) The sedimentation.

5.1 Sea level and sedimentary trends.

The cycles described before record a complete oscillation from flooding (deepening) to drying (shallowing) that can be explained through these parameters.

The lower part of the cycle implies that the water level is increasing in relation to the marsh bottom. This creation of accommodation space can be achieved by sinking the bottom of the marsh (subsidence) or rising the base level (sea level). In both cases, the relative sea level rise must be higher than the infill by sediments, that reduces the accommodation space, and results in successively deeper facies being deposited (Fig. 5a). As faster the sea level rise vs. the sedimentation rate is, the thinner the sequence is.

The shallowing sequence indicates that the rate of creation of accommodation space is slower than rate of its destructive mechanisms. This can be the result of slower or negative rates of sea level rise, increase in sedimentation rate or uplift of the bottom of the marsh. The resulting sequence is composed by progressively shallower facies (Fig. 5b). As more similar the rates of sea level rise and sedimentation are, the thicker the sequence is.

Thus, the cycles recorded in the marsh sediments record a whole cycle of sea level (Fig. 5c): a flooding-deepening sequence (sea level rise) followed by a drying-shallowing sequence (sea level stable and/or falling) that reaches its lowest point at the cycle boundary.

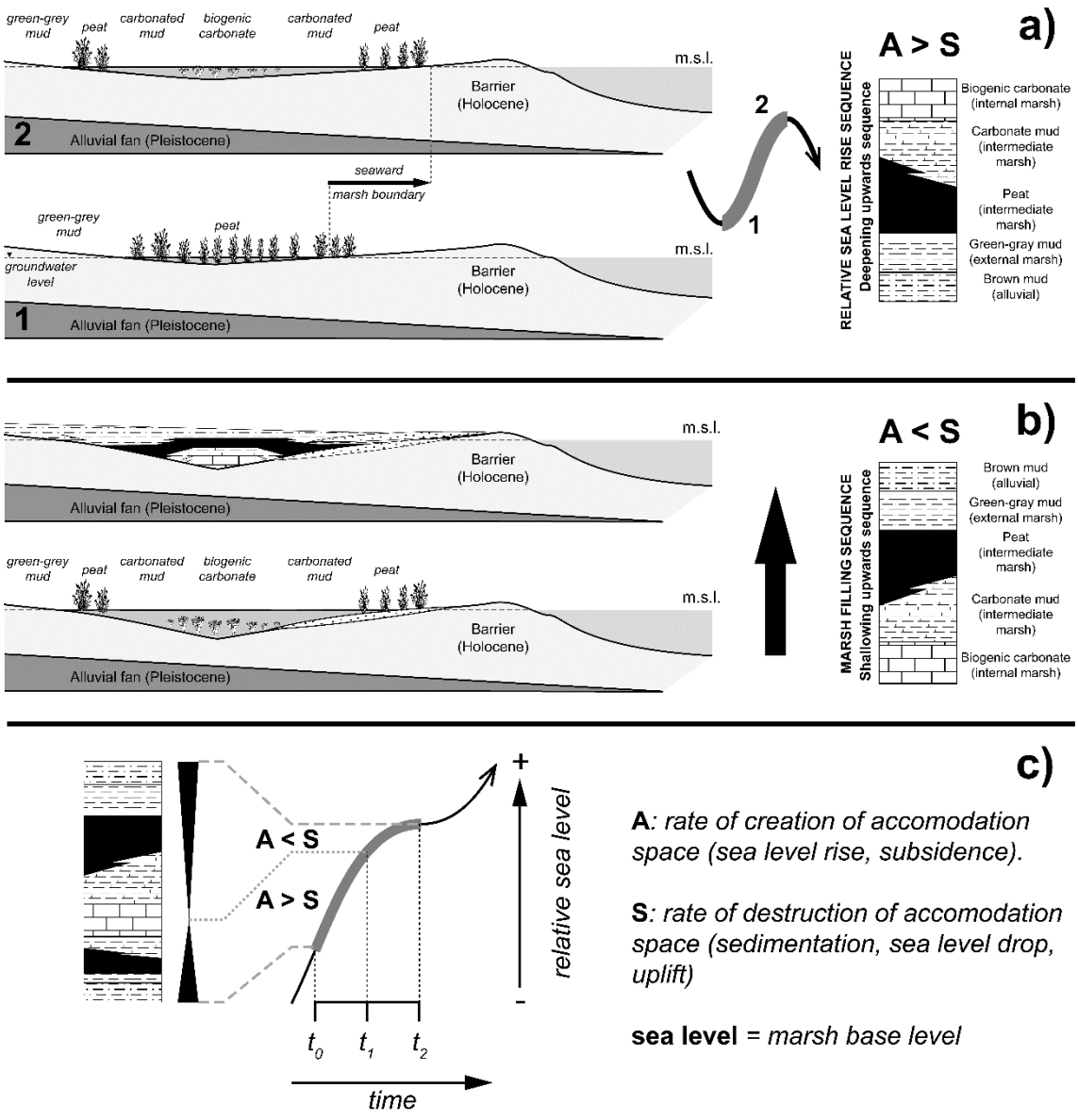

Figure 5. *Conceptual model of the deepening-shallowing cycle. a) Deepening sequence resulting from sea level (base level) rise not balanced by sedimentation (A>S). b) Shallowing sequence as result of sedimentation rate greater than rate of sea level rise (A<S), c) Cycle development as consequence of changes in the rate of relative sea level rise.*

5.2 Correlation of sea level changes and chronological implications.

The correlation of such sequences between both marshes seems to confirm that they are not due to specific effects of the wetland itself (i.e., permeability of the coastal ridge, subsidence, ...) but to regional scale processes.

Vacchi et al. (2018) determine that sea level rose in the Gulf of Valencia around 0.9 m during the last 4.8 ka while in the Balearic Islands it was 1.5 m since 6 ka BP. For the coast of Catalonia (N Mediterranean Spanish coast), they establish a sea level rise of 2.6 m for the last 4.6 ka and 0.8 m since 2 ka BP.

Despite these authors consider that the data of the Gulf of Valencia are affected by subsidence, there are differences among the data from Valencia, Albufera de Valencia (Valencia lagoon) and those from Almenara. While the first ones show an initial fall of sea level followed by a rise until present day, the data from Almenara indicate a more stable sea level that can be compared to the Ebro Delta subsidence-corrected curve (Somoza et al., 1998) and those from the Gulf of Almería (Goy et al., 2003) (Fig. 6).

Goy et al. (2003) determine that, for the last 6000 years, the range of the sea level oscillation was about 1.2 m in the Gulf of Almería (S Mediterranean Spanish coast).

Albufereta marsh record, located southwards of our study area, shows a rise in sea level until around 3 ka. BP (Ferrer and Blázquez, 2016) and, afterwards, cyclic (200-400 years) centimetre scale relative sea level fluctuations that could be related to the increase of low pressure systems in the Mediterranean basin (Zazo, 2006).

A major marine incursion is recorded around 3-2.5 ka BP in the coastal barrier-lagoon of Valencia (Ruiz-Pérez and Carmona, 2019). They also identify sand spit formation episodes at 2.9-2.2 ka BP and 1.5-1.2 ka BP and beach barrier progradation from 1.1 ka BP until recent times. For the same system, López-Belzunce et al. (2020) place sea level at -1.2 m below sea level (b.s.l.) at 3 ka BP, -1 m b.s.l. at 2 ka BP and at 0.4 m b.s.l. at 1 ka BP (Fig. 6). However, these authors consider that sea level influence was minor for the last 2.8 ka.

In the Almenara marsh, Blázquez et al. (2018) determine that from ca. 4820 yr BP onwards the oligohaline marsh was relatively stable with marine influence.

In any case, the recorded range of sea level change was below 2 meters for the last 4000 years, what is near the thickness of our cycles, implying a minor contribution of subsidence in this area. It also implies, that main changes in the coastline position (progradation/retrogradation) should have been related to changes in sediment supply than to sea level change.

The comparison of our cycles and dates to curves of reconstructed sea level is also useful to precise the chronological scheme down to ca. 5.5 ka BP (Fig. 6).

For cycle 3, its base is younger than 5.6 ka BP (cycle 4). This is near the d1-a2 transition (ca. 5.6 ka BP) of the Ebro Delta (Somoza et al., 1998) and it is coherent with the sudden change ca. 5.4 ka BP in the Almenara marsh (Vacchi et al., 2018), and correlative to the bottom of the H2 prograding unit (5.4 ka BP) at the Gulf of Almería (Goy et al., 2003). Consequently, an age of ca. 5.4 ka BP can be assigned to this boundary.

The maximum flooding surface of this cycle should be older than 4-4.2 ka BP and younger than 5.4 ka BP. Somoza et al. (1998) place the h2 relative highstand at 5.2 ka BP but Vacchi et al. (2018) show a relative high sea level at 4.8 ka BP at the Almenara marsh. There is no conclusive information from the Gulf of Almería so the last date (ca. 4.8 ka BP) is accepted for this flooding surface.

For cycle 2, its base must be younger of 4 ka BP. It could be correlative to the d2-a3 transition that can be placed ca. 4 ka BP (Somoza et al., 1998). Data from the Valencia show a relative low sea level position ca. 3.8 ka BP (no information for the Almenara marsh) (Vacchi et al., 2018) that is very similar to the ca. 3.9 ka BP age of the beginning of the erosive period inside the H3 prograding unit of the Gulf of Almería (Goy et al., 2003). Thus, an age of ca. 3.8 ka BP is assigned to the base of cycle 2.

The maximum flooding surface for this cycle is younger than 3.5 ka BP. h3 relative highstand for Ebro Delta has been dated as 3.3 ka BP (Somoza et al., 1998) and data from the Albufera de Valencia (Valencia lagoon) show a relative high level around 3.5 ka BP (Vacchi et al., 2018). For the Gulf of Almería these dates are encompassed in the 3.2-3.9 ka BP erosive gap inside the H3 prograding unit. Therefore, a ca. 3.4 ka BP age is assumed for this flooding surface.

Chronological location of cycle 1 is more complex as there are no dates between the flooding surfaces of cycle 1 and cycle 2. The absence of evident stratigraphic gaps (absence of erosive surfaces, continuity in the sedimentary style and facies) is a criterion to assign chronological information to cycle 1.

Assuming this continuity, cycle 1 should be equivalent to the a4 to a5 lapse for the Ebro Delta (Somoza et al., 1998). For that area, after the agradational unit (a4), the three-fold relative highstand (h4), together with the d1 and a5 units, show a progressive rise of relative sea level but with lower rates than for previous units (drop of sea level for the subsidence-corrected curve). This is compatible with the shallowing sequence of cycle 1 that finishes with terrestrial deposits.

The base of this cycle is then correlated to the end of the d3 prograding unit of Ebro Delta (ca. 2.8 ka BP. In the Albufera de Valencia, a low sea level is recorded ca. 2.9 ka BP (Vacchi et al., 2018) and for the Gulf of Almería there is a lacuna between the H3 and H4 prograding units (linked to a sea level fall) between 2.7 and 3 ka BP (Goy et al., 2003). On that basis, the base of cycle 1 is assigned to ca. 2.8 ka BP.

The highest level (flooding surface) for this cycle is younger than 0.7 ka BP. Relative highstands for this period are dated as 2.3 ka BP (h4a), 1.8 ka BP (h4b) and 1.2 ka BP (h4c). Data for the Almenara marsh shows a noticeable rise in sea level from 2 ka BP until 1.8 ka BP (Vacchi et al., 2018). This date is near the 1.9 ka BP age for the boundary between the H4 and H5 prograding units of the Gulf of Almería, that is related to high sea level (Goy et al., 2003). Following this reasoning, an age of ca. 1.8 ka BP is assigned to the flooding surface of cycle 1.

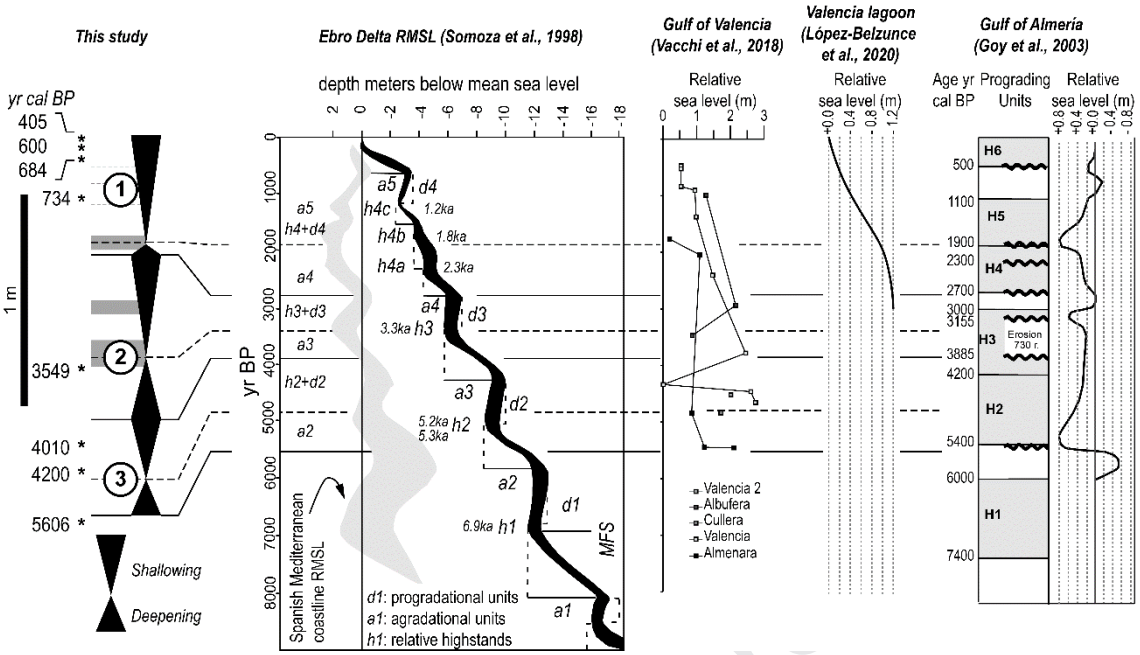

Figure 6. Correlation of sedimentary cycles for the Almenara marsh and sea level changes at different locations of the Spanish Mediterranean coast.

5.3. Salinity: climate vs. sea level change.

Sea level oscillations modify the position of the base level of the marshes, but also control the displacements of the boundary between the groundwaters of marine and terrestrial origin.

Changes in sea level and in sedimentation rates in the coast are responsible for the progradation or retrogradation/erosion of the beach deposits causing variations in the distance from the marsh (mostly static in time) to the shoreline (mostly changing).

Changes in sedimentation rates at the shore can be related to different factors (availability of sources, water discharge, gradients, wind and currents, etc.) but, simplifying, the main factor is the supply of sediment from rivers. The amount of sediment depends on water discharge from rivers and this, in turn, can be related to rainfall.

Thus, sea level and climate control the position of the marine/terrestrial groundwaters boundary and, finally. the composition of the waters of the wetland.

For decennial to centennial time scales (Fig. 7), during wet periods there is an increase of sediment supply to the coast that favours the growth of beaches preventing their retreat or promoting their progradation. Consequently, the boundary of the marine-terrestrial groundwaters is displaced away from the marsh and the supply of saline elements is reduced. Additionally, the increase in rainfall will fed the terrestrial groundwaters and increase in surface runoff will led to greater inputs of freshwater to the marsh.

If the sea level is stable the surface of the marsh will stay at the same position but the increase in runoff will supply higher quantities of siliciclastics (Si, Al).

If the sea level is falling then surface of the marsh will decrease as consequence of a falling base level; progradation of the marginal vegetation fringe and marginal areas towards the centre of the marsh will result in an increase in siliciclastics (Si, Al) and organic matter (organic C).

However, if sea level is rising and sedimentation rate is high enough to prevent beach retrogradation, the wetland will deepen due to the base level rise and freshwater inputs. Consequently, bioinduced carbonate (Ca, inorganic C) will increase and the waters will be oxygenated (Mn/Fe increase).

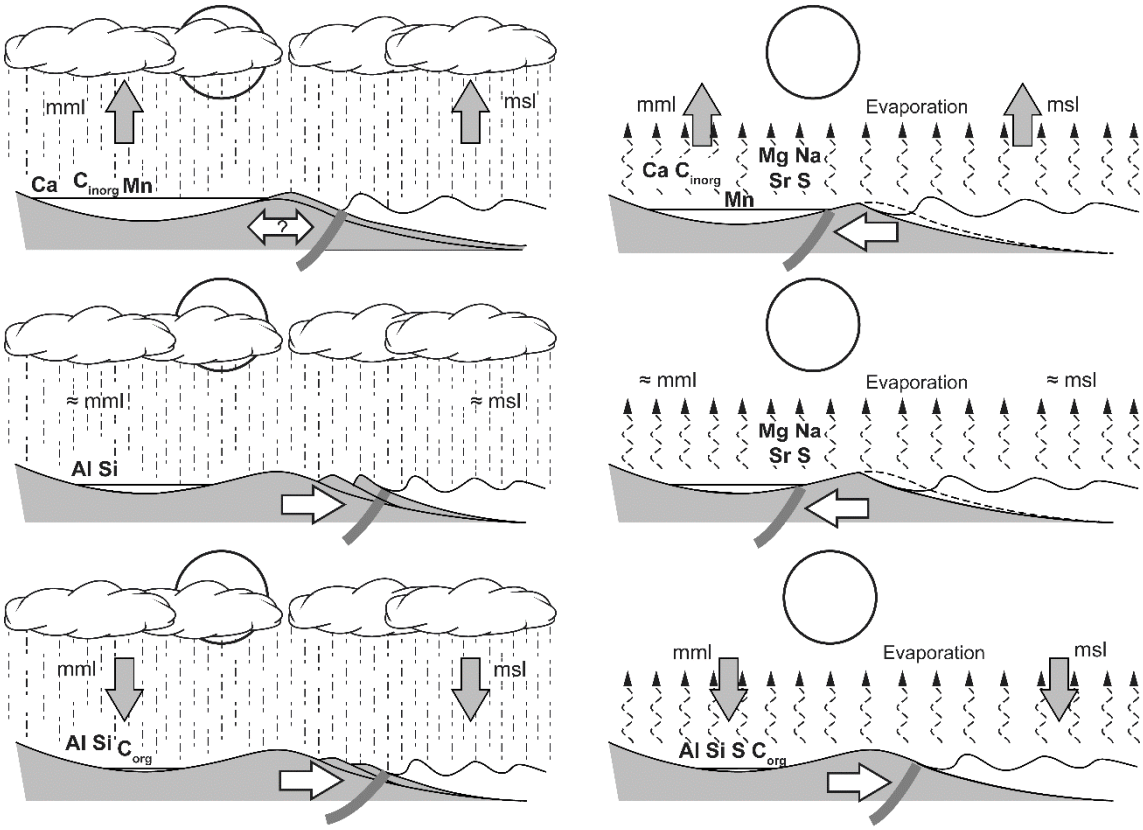

mml: mean marsh level / msl: mean sea level

Figure 7. *Conceptual model for the sea level and climate relation to geochemical composition. Big arrows point to the displacement of the water levels. The depicted elements increase for the conditions depicted in each sketch. Upper row: rising sea level; middle row: stable sea level; lower row: falling sea level. Left column: wet periods; right column: arid periods. Thick line: boundary of marine-terrestrial groundwater (MTGB); white arrow: sense of displacement of the MTGB.*

During arid periods, the supply of sediment to the coast will decrease, favouring the erosion of beaches or not allowing their growth. In addition, increased evaporation will promote the rise of salinity.

For stable sea level periods, the shoreline will move landwards due to the decrease of sediment supply. This will cause the displacement of the marine-terrestrial groundwaters towards land, increasing the flux of saline elements of marine origin towards the marsh and increasing the salinity of the marsh waters by evaporative processes (Mg, Na, S, Sr).

For falling sea level stages, the shoreline can displace seawards together with the marine-terrestrial groundwater boundary. This will decrease the flux of saline elements from the sea. In addition, the water depth and extent will drop as the base level falls. As a consequence, the marginal environments (alluvial, external marsh, peat) will occupy inner positions (Al, Si, organic C) and salinity will increase by evaporation of mainly terrestrial waters (S).

If sea level rises, the deficit of sediment will promote beach erosion, landward displacement of the shoreline, while, simultaneously, the marsh level will rise following the base level (deepening). The marine-terrestrial groundwater boundary will move landwards causing the salinization of the marsh waters. The deepening and flux of groundwater will led to the sedimentation of bioinduced carbonate (Ca, inorganic C) and oxygenated waters (higher Mn/Fe ratio) but the marine origin of these waters and increased evaporation will result in an increase in salinity (Mg, Na, Sr, S).

But, in addition to the control by climate and sea level, there are also differences that can be related to the environmental position of the cores. The smaller salinity pulses record minor sea intrusion events that are more evident in C3 while in C7 and C10 these pulses show some freshwater influence as recorded by the decrease in Na. This can be related to the location of the cores. While C3 is placed near the sea (high Si/Al and low Al values, representing a source near the shore) and far from the course of the main rivers, C10 is placed landwards, near the toe of alluvial cones (high Al and intermediate Si/Al values), and C7 is in the area of influence of the surface and groundwaters of the Palancia river (the main fluvial system supplying siliciclastics, high Al and Si/Al values). Consequently, C3 is dominated by the marine dynamics while C7 and C10 show a better record of terrestrial floods.

These facts are also responsible of the similitudes and differences of the cycles among cores. All of them show two main salinity pulses in the lower sequence (deeper facies) that can be easily correlated and represent small sea level fluctuations that were counterbalanced by freshwater inputs from land in C7 and C10.

Also, there is an in average difference among cycles. Cycle 2 is more saline than cycle 1 and this can be related to the greater influence of terrestrial inputs (as recorded by the greater representativity of alluvial facies) as consequence of the filling and continentalization of the marsh.

5.4. Salinity events and climate variability

The salinity episodes recorded in the Almenara marsh show no chronological relation to the environmental changes recorded in other coastal wetlands of the Spanish Mediterranean coast (Fig. 8). But this is a common feature all along the Mediterranean coast, the lack of synchronicity of these changes.

However, these salinity episodes are coeval to periods of lower activity of the Turia river what it is related to the lower or no growth of the coastal barrier. This points to drier conditions than during the other periods.

As compared to other aridity records in the Iberian Peninsula, the recorded episodes are synchronous with drier periods recorded in pollen sequences from the Alborán Sea (Fletcher et al., 2013).

The salinity episode ca. 3.4 ka BP is coetaneous to low lake level in Lake Zoñar (S Spain, Martínez-Puertas et al., 2008), but not to records from other areas, like Lake Siles (Carrión, 2002) and Laguna de Medina (Reed et al., 2001) in S Spain. Fluvial systems were active, but less than during the last two millennia.

The ca. 3 ka BP salinity episode correlates to dry phases in Lake Siles, Lake Zoñar and two dessication events in Laguna Medina bracket this period. Fluvial activity was lower than during the previous dry period and lake levels in central Europe were clearly lower than during the preceding and following times (Magny, 2004).

Coincidences with aridity records for the 1.8 ka BP period are more abundant. An exception is Lake Zoñar, but this can be due to chronological issues. However, like for the 3.4 period, lake levels in central Europe were not lower but neither high (Magny, 2004).

These facts seem to indicate that these salinity episodes were coincidental with low fluvial activity periods and low lake levels or dry conditions, being the ca. 3 ka BP episode the driest.

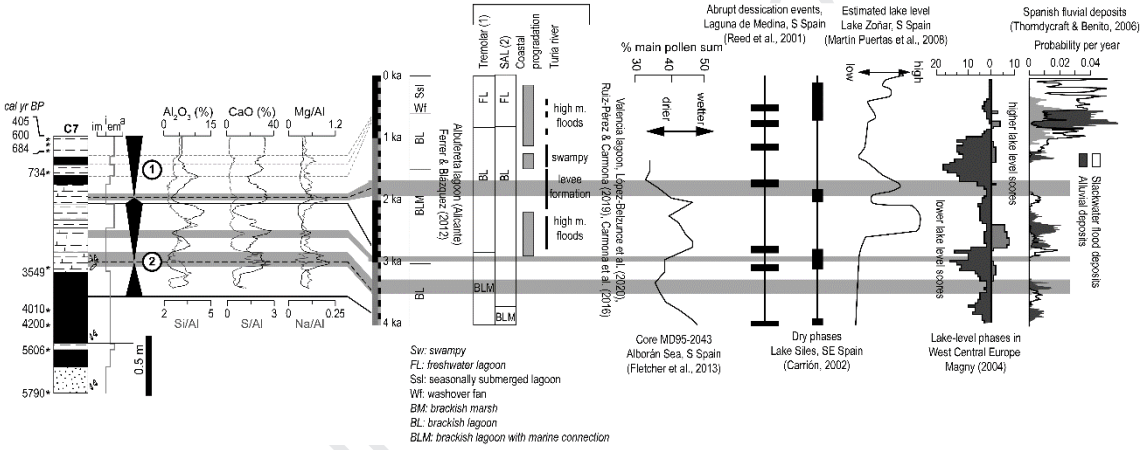

Figure 8. *Comparison of salinity periods to environmental evolution of nearby coastal lagoons, aridity records in marine and terrestrial Spanish areas, lake levels in central Europe and fluvial activity in Spain.*

On a broader scale (Fig. 9), these salinity episodes are coincidental with times of more frequent dry periods (Wanner et al., 2011). But there is no clear relation to paleoceanographic reconstructions for the Western Mediterranean. Reconstructions for the Alborán Sea (Rodrigo-Gámiz et al., 2014; Cacho et al., 1999) and the Balearic Sea (Cisneros et al., 2016) are not coincidental and, beyond the overall trend to falling SST until present, the salinity episodes are correlative to small falls in SST. However, the correlation to higher resolution reconstructions for the North Atlantic Ocean (i.e. Bond et al., 2001; Sejdrup et al., 2011) is better and the salinity episodes are clearly coetaneous of cooler SST periods.

These episodes took place during periods dominated by positive anomalies of the North Atlantic Oscillation (NAO) (Olsen et al., 2012) but correspond to short events of falling values during these periods.

A similar behaviour is observed in relation to the solar activity. The salinity/aridity episodes took place during short events of slightly falling values of Total Solar Irradiance (Steinhilber et al., 2012) or lower sunspot numbers (Solanki et al., 2004), but not during the lowermost ones.

Summarizing, the recorded episodes correspond to drier periods that occurred coeval to lower SST pulses, short falling events during positive NAO periods and short and low falls in solar activity.

These facts point to the relation of these events to processes acting on short time scales (decennial to centennial). Thus, small changes in solar activity could have caused small falls in SST that could have lowered the evaporation of the marine waters. And the displacement of the storm tracks as result of neutral to positive values of the NAO would have increased the dry conditions.

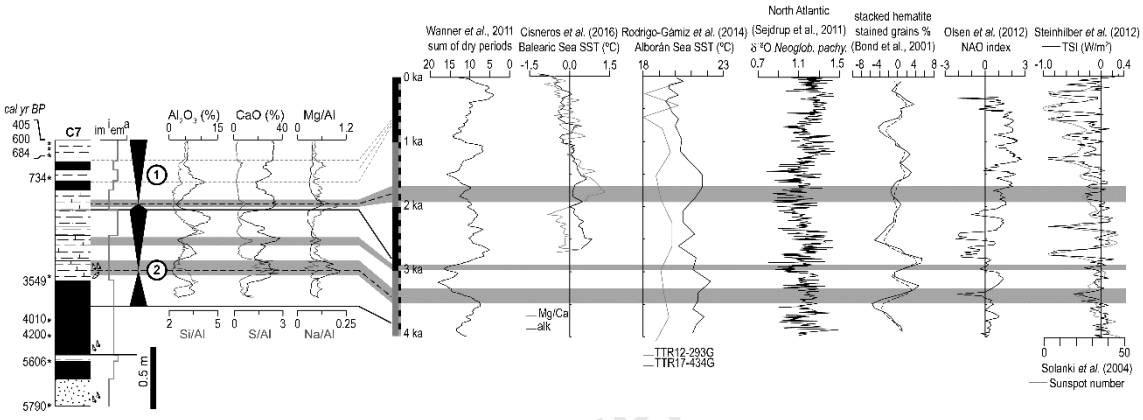

Figure 9. *Salinity/aridity episodes and their comparison to global dry periods, paleoceanographic (SST), atmospheric (NAO index) and solar (Total Solar Irradiance and sunspot numbers).*

6. Conclusions

The geochemical and facies record for the last 4000 years of three cores from Mediterranean marshes allows to identify short salinity records resulting from the joint effect of sea level and climate. In addition, sequence stratigraphy and correlation to regional sea level curves have allowed to improve the chronology of such deposits.

Their water level and quality are related to the balance between the marine and terrestrial waters via surface and groundwater flows which, in turn, depend on the marine water front position (sea level and distance to the coast) and the terrestrial water budget. During wet periods, the supply of sediments from rivers enhances the progradation of the beaches displacing the saline marine water front seawards. But during dry periods, displacement of the marine water front landwards due to the erosion of the coastal deposits during stable or rising sea level periods increases the salinity of the water, which is raised by the higher evaporation rates.

Three episodes (ca. 3.4 ka BP, ca. 3 ka BP and ca. 1.8 ka BP) of higher salinity have been identified inside the in overall dry conditions for the last 4000 years.

In addition to the conceptual model, comparison to other local, regional and global records, allows to correlate these episodes to periods of drier conditions. When analysed these results, the observed changes in the sediments result from minor oscillations in forcings (SST, NAO, solar activity) that were amplified by the environmental processes.

Acknowledgements

This work has been funded by the Geological Survey of Spain. Particularly, J.F. Mediato acknowledges predoctoral funding from Spanish Geological Survey. The authors a grateful to the Guest Editor of this volume, Prof. Alejandro Cearreta, and the Main Editor of Quaternary International, Dr. Thijs van Kolfschoten. Special thanks are also due to Pedro J.M. Costa and an anonymous reviewer whose helpful comments and suggestions have improved a lot this manuscript.

References

Blázquez-Morilla, A.M., Rodríguez-Pérez, A., Sanjuán-Lamata, D. (2018). Palaeoenvironmental evolution from the early Holocene to the present of the Almenara marsh (western Mediterranean). Scientia Marina, 82, 257-268. https://doi.org/10.3989/scimar.04853.07A

Blázquez, A.M., Rodríguez-Pérez, A., Torres, T., Ortiz, J.E., 2017. Evidence for Holocene sea level and climate change from Almenara marsh (Western Mediterranean). Quat. Res. 88: 206-222. https://doi.org/10.1017/qua.2017.47

Bond, G., Kromer, B., Beer, J., Muscheler, R., Evans, M.N., Showers, W., Hoffman, S., Lotti-Bond, R., Hajdas, I., Bonani, G., 2001. Persistent solar influence on north Atlantic climate during the Holocene. Science 294, 2130-2136.

Cacho, I., Grimalt, J.O., Pelejero, C., Canals, M., Sierro, F.J., Flores, J.A., Shackleton, N., 1999. Dansgaard-Oeschger and Heinrich event imprints in Alboran Sea paleotemperatures. Paleoceanography, 14, 6, 698-705.

Calvert, S.E., Pedersen, T.F., 2007. Elemental Proxies for Palaeoclimatic and Palaeoceanographic Variability in Marine Sediments: Interpretation and Application. In: Hillaire-Marcel, C., De Vernal. A. (Eds.), Proxies in Late Cenozoic Paleoceanography, Developments in Marine Geology, 1, Elsevier, pp. 567-644.

Carmona, P., Ruiz, J.M., 2011. Historical morphogenesis of the Turia River coastal flood plain in the Mediterranean littoral of Spain. Catena 86(3): 139–149.

Carmona, P., Ruiz-Pérez, J.-M., Blázquez, A.M., López-Belzunce, M., Riera, S., Orengo, H. 2016. Environmental evolution and mid–late Holocene climate events in the Valencia lagoon (Mediterranean coast of Spain). The Holocene, 26, 1750-1765. https://doi.org/10.1177/0959683616645940

Carrión J.S., 2002. Patterns and processes of Late Quaternary environmental change in a montane region of southwestern Europe. Quat. Sci. Rev. 21, 2047-2066.

Cisneros, M., Cacho, I., Frigola, J., Canals, M., Masqué, P., Martrat, B., Casado, M., Grimalt, J.O., Pena, L.D., Margaritelli, G., Lirer, F., 2016. Sea surface temperature variability in the central-western Mediterranean Sea during the last 2700 years: a multi-proxy and multi-record approach. Climate of the Past, 12, 849-869.

Corella, J.P., Stefanova, V., El Anjoumi, A., Rico, E., Giralt, S., Moreno, A., Plata-Montero, A., Valero-Garcés, G.L., 2013. A 2500-years multy-proxy reconstruction of climate change and human activities in nothern Spain: The Lake Arreo record. Palaeogeog. Palaeoclimatol. Palaeoecol. 386, 555-568. http://dx.doi.org/10.1016/j.gr.2013.06.022.

Dupré, M., Fumanal, M.P., Sanjaume, E., Santisteban, C. Usera, J. Viñals, M.J., 1988. Quaternary evolution of Pego coastal lagoon (Southern Valencia, Spain). Paleogeog. Paleoclimatol. Paleoecol. 68: 291-299. https://doi.org/10.1016/0031-0182(88)90046-6

Engstrom, D.R., Hansen, B.C.S., 1985. Postglacial vegetational change and soil development in southeastern Labrador as inferred from pollen and chemical stratigraphy. Can. Jour. of Bot., 63, 543-561.

Ferrer García, C., Blázquez Morilla, A.M. 2012. The Evolution of the Albufereta Lagoon (Western Mediterranean): Climate Cycles and Sea-Level Changes. Jour. of Coastal Res., 28, 1617-1626.

Fletcher, W.J., Debret, M., Sanchez Goñi, M.F., 2013. Mid-Holocene emergence of a low-frequency millennial oscillation in western Mediterranean climate: Implications for past dynamics of the North Atlantic atmospheric westerlies. The Holocene 23, 153-166.

Fontboté, J.M., Guimerà, J., Roca, E., Sàbat, F., Santanach, P. Fernández-Ortigosa, F. 1990. The Cenozoic geodynamic evolution of the Valencia trough (Western Mediterranean). Rev. de la Soc. Geol. de Esp. 3, 249-259.

Fullana, J. 2001. Plan de protección de recursos hídricos de la zona húmeda de Almenara. Dirección General de Obras Hidráulicas y Calidad de las Aguas. Ministerio de Medio Ambiente, Oficina de Planificación Hidrológica, 226 pp.

Giménez, E., 1994. Caracterización hidrogeoquímica de los procesos de salinización en el acuífero detrítico costero de la Plana de Castellón (España). Ph.D. thesis. Universidad de Granada. 469 pp.

Giménez. E., Morell, I. 1997. Hydrogeochemical analysis of salinization processes in the coastal aquifer of Oropesa (Castellón, Spain). Envir. Geol., 29, 118-131.

Giralt, S., Moreno, A., Cacho, I. Valero-Garcés, B., 2017. A comprehensive overview of the last 2,000 years Iberian Peninsula climate history. CLIVAR Exchanges,73. Special Issue on climate over the Iberian Peninsula: an overview of CLIVAR-Spain coordinated science. DOI: https://doi.org/10.31978/639-18-002-5.02

Goy, J.L., 1978. Estudio Geomorfológico del Cuaternario Litoral Valenciano. Ph.D. thesis. Universidad Complutense de Madrid.

Goy, J.L., Zazo, C., Dabrio, C.J., 2003. A beach-ridge progradation complex reflecting periodical sea-level and climate varibility during the Holocene (Gulf of Almería, Western Mediterranean). Geom. 50, 251-268. DOI:10.1016/S0169-555X(02)00217-9

López-Belzunce, M., Blázquez, A.M., Carmona, P., Ruiz, J.M. (2020). Multi proxy analysis for reconstructing the late Holocene evolution of a Mediterranean Coastal Lagoon:

Environmental variables within foraminiferal assemblages. Catena, 187, 104333 https://doi.org/10.1016/j.catena.2019.104333

Mackereth, F.J.H. 1966. Some chemical observations on post-glacial lake sediment. Philos. Trans. of the Royal Soc. of Lond., Series B, Biological Sciences, 250, 165-213.

Magny, M., 2004. Holocene climate varibility as reflected by mid-European lake-level fluctuations and its probable impact on prehistoric human settlements. Quat. Inter., 113, 65-79.

Marco-Barba, J., Holmes, J.A., Mesquita-Joanes, F., Miracle, M.R., 2013. The influence of climate and sea-level change on the Holocene evolution of a Mediterranean coastal lagoon: Evidence from ostracod palaeoecology and geochemistry. Geobios, 46, 409-421.

Martín-Puertas, C., Valero-Garcés, B.L., Mata, M.P., González-Sampériz, P., Bao, R., Moreno, A., Stefanova, V., 2008. Arid and humid phases in southern Spain during the last 4000 years: the Zoñar Lake record, Córdoba. The Holocene 18, 907-921.

Martin-Vide, J. 1997. Avances en climatología histórica en España. Oikos-Tau, Barcelona, 223 pp.

Mediato, J.F., 2016. Oscilaciones del nivel del mar desde el Pleistoceno superior en el sector costero Sagunto-Benicasim (Valencia- Castellón). Registro sedimentario, geoquímico e histórico. Ph.D. thesis. Universidad Complutense de Madrid, Madrid.

Mediato, J.F., Medialdea, A., Mediavilla, R.M., Salazar, A., Santisteban, J.I., Perucha, M.A., Dabrio C.J., 2015. Dataciones por luminiscencia de los depósitos aluviales y deltaicos de la llanura costera de Castellón. Implicaciones paleogeográficas. In. Una visión global del Cuaternario. El hombre como condicionante de procesos geológicos. (J. P. Galve, J. M. Azañón, J. V. Pérez Peña y P. Ruano, Eds.). XIV Reunión Nacional de Cuaternario, Granada (España). pp. 33-37

Mediato, J.F., Santisteban, J.I., 2006. Subfacies geoquímicas: una mejora en la caracterización de depósitos litorales (sondeo de Almenara, provincia de Castellón). Bol. Geol. y Min. (Núm. Monográfico Especial) 117: 519–524.

Mediavilla, R., Santisteban, J.I., Mediato, J.F., 2013. El registro sedimentario del Holoceno en el Parque Nacional de Las Tablas de Daimiel. In: Mediavilla, R., Instituto Geológico y Minero de España, Serie: Medio Ambiente (Eds.), Las Tablas de Daimiel: Agua y sedimentos. Publicaciones del. vol. 14. IGME, Madrid, pp. 169–186.

Montón, E., Quereda, J., 1997. ¿Hacia un cambio climático? La evolución del clima mediterráneo desde el siglo XIX. Fundación Davalos Fletcher, Castellón, 520 pp.

Morellón, M., Valero-Garcés, B., González-Sampériz, P., Vegas-Vilarrúbia, T., Rubio, E., Rieradevall, M., Delgado-Huertas, A., Mata, P., Romero, Ó., Engstrom, D. R., López-Vicente, M., Navas, A., Soto, J., 2011. Climate changes and human activities recorded in the sediments of Lake Estanya (NE Spain) during the Medieval Warm Period and Little Ice Age. Jou. of Paleol., 46, 423-452. doi:10.1007/s10933-009-9346-3.

Morell, I., Giménez, E., Esteller, M.V. 1996. Application of principal components analysis to the study of salinization on the Castellon Plain (Spain). The Sci. of the tot. Envir., 177, 161-171.

Olsen, J., Anderson, N.J., Knudsen, M.F., 2012. Variability of the North Atlantic Oscillation over the past 5,200 years. Nat. Geos, 5, 808-812.

Ramos-Román, M.J., Jiménez-Moreno, G., Camuera, J., García-Alix, A., Anderson, R.S., Jiménez-Espejo, F.J., Sachse, D., Toney, J.L., Carrión, J.S., Webster, C., Yanes, Y., 2018. Millennial-scale cyclical environment and climate variability during the Holocene in the western Mediterranean region deduced from a new multiproxy analysis from the Padul record (Sierra Nevada, Spain). Glob. Planet. Chang. 168, 35–53. https://doi.org/10.1016/j.gloplacha.2018.06.003

Reed, J.M., Stevenson, A.C., Juggins, S., 2001. A multi-proxy record of Holocene climatic change in south-western Spain: the Laguna de Medina, Cádiz. The Holocene 11, 707-719.

Reimer, P.J., Bard, E., Bayliss, A., Beck, J.W., Blackwell, P.G., Bronk Ramsey, C., Buck, C.E., Cheng, H., Edwards, R.L., Friedrich, M., Grootes, P.M., Guilderson, T.P., Haflidason, H., Hajdas, I., Hatte, C., Heaton, T.J., Hoffmann, D.L., Hogg, A.G., Hughen, K.A., Kaiser, K.F., Kromer, B., Manning, S.W., Niu, M., Reimer, R.W., Richards, D.A., Scott, E.M., Southon, J.R., Staff, R.A, Turney, C.S.M., van der Plicht, J., 2013. IntCal13 and Marine13 radiocarbon age calibration curves 0-50,000 years cal BP. Radiocarbon. 55, 1869–1887.

Roca, E. 2001. The northwestern mediterranean basin (Valencia trough, Gulf of Lions and Liguro-Provençal basins): Structure and geodynamic evolution. En: Ziegler P.A., Cavazza W., Robertson A.H.F. y Crasquin-Soleau S. (Eds.): Peri-Tethys Memoir 6: Peri-Tethyan rift-Wrench basins and passive margins. Memoires du Museum National d`Histoire Naturelle de Paris, 186, 671-706.

Rodrigo-Gámiz, M., Martínez-Ruiz, F., Rampen, S.W., Schouten, S., Sinninghe Damsté, J.S., 2014. Sea surface temperature variations in the western Mediterranean Sea over the last 20 kyr: A dual-organic proxy ($U^{K'}_{37}$ and LDI) approach. Paleoceanography, 29, 87-98, doi:10.1002/2013PA002466

Rodríguez-Pérez, A., Blázquez, A.M., Guillem, J., Usera, J., 2018. Maximum flood area during MIS 1 in the Almenara marshland (western Mediterranean): Benthic foraminifera and sedimentary record. Holocene. 28: 1452-1466. https://doi.org/10.1177/0959683618777069

Ruiz-Pérez, J.M, Carmona P., 2019. Turia river delta and coastal barrier-lagoon of Valencia (Mediterranean coast of Spain): Geomorphological processes and global climate fluctuations since Iberian-Roman times. Quat. Sci. Rev. 219, 84-101. https://doi.org/10.1016/j.quascirev.2019.07.005

Ruiz-Zapata, M.B., Gil-García, M.J., Bustamante, I., 2010. Paleoenvironmental reconstruction of Las Tablas de Daimiel and its evolution furing the Quaternary Period. In: Sánchez-Carrillo S. y Angeler D.G. (Eds.): Ecology of Threatened Seimi-Arid Wetlands Long-Term Research in Las Tablas de Daimiel. Springer, 23-43.

Santisteban, J.I., Mediavilla, R, Galán de Frutos, L. López Cilla, I., 2019. Holocene floods in a complex fluvial wetland in central Spain: Environmental variability, climate and time. Glob. Planet. Chang. 181, 102986. https://doi.org/10.1016/j.gloplacha.2019.102986

Simón, J.L., 1984. Compresión y distensión alpinas en la Cadena Ibérica Oriental. Instituto de Estudios Turolenses (CSIC), Teruel, 269 pp.

Sejrup, H.P., Haflidason, H., Andrews, J.T., 2011. A Holocene North Atlantic SST record and regional climate variability. Quarter. Scien. Rev., 30, 3181-3195.

Solanki, S. K., Usoskin, I. G., Kromer, B., Sch¨ussler, M., Beer, J. 2004. Unusual activity of the Sun during recent decades compared to the previous 11,000 years. Nature, 431, 1084–1087. https://doi.org/10.1038/nature02995.

Somoza, L., Barnolas, A., Arasa, A., Maestro, A., Rees, J.G., Hernández-Molina, F.J. 1998. Architectural stacking patterns of the Ebro delta controlled by Holocene high-frequency eustatic fluctuations, delta-lobe switching and subsidence processes. Sedim. Geol., 117, 11-32.

Steinhilber, F., Abreu, J.A., Beer, J., Brunner, I., Christl, M., Fischer, H., Heikkilä, U., Kubik, P.W., Mann, M., McCracken, K.G., Miller, H., Miyahara, H., Oerter, H., Wilhelms, F., 2012. 9,400 years of cosmic radiation and solar activity from ice cores and tree rings. Proceedings of the National Academy of Sciences, 109, 5967-5971.

Stuiver, M., Reimer, P.J., 1986. A computer program for radiocarbon age calibration. Radiocarbon 28, 1022–1030.

Stuiver, M., Reimer, P.J., 1993. Extended 14C database and revised CALIB radiocarbon calibration program. Radiocarbon 35, 215–230.

Stuiver, M., Reimer, P.J., Reimer, R., 2015. CALIB Radiocarbon Calibration Version 7.1. Available at: http://calib.qub.ac.uk/calib/.

Thorndycraft, V., Benito, G., 2006. Late Holocene fluvial chronology in Spain: The role of climatic variability and human impact. Catena, 66, 34-41.

Tuñón J. (2000): Determinación experimental del balance hídrico del suelo y evaluación de la contaminación asociada a las prácticas agrícolas. Ph. D. Thesis. Departamento de Ciencias Experimentales, Universitat Jaume I, Castellón. 367 pp.

Usera, J., Blázquez, A.M., Guillem, J., Alberola, C., 2002. Biochronological and paleoenvironmental interest of foraminifera lived in restricted environments: application of to the study of the western Mediterranean Holocene. Quat. Inter. 93-94, 139-147.

Usera, J., López Buendía, A., Alberola, C., 1996. Foraminíferos cuaternarios de la turbera de Benicasim (Castellón). XII Bienal Real Soc. Esp. la de His. Nat. 200, 24.

Vacchi, M., Ghilardi, M., Melis, T.R., Spada, G., Giaime, M., Marriner, N., Lorscheid, T., Morhange, C., Burjachs, F., Rovere, A. (2018). New relative sea-level insights into the isostatic history of the Western Mediterranean. Quaternary Science Reviews, 201, 396-408.

732 Vegas, R., de Vicente, G. 2004. El Surco de Valencia. En: Vera J.A. (Ed.): Geología de
733 España SGE-Instituto Geológico y Minero de España, Madrid, 274-276.

734 Viñals, M.J., Fumanal, M.P., 1995. Quaternary development and evolution of the
735 sedimentary environments in the central mediterranean spanish coast. Quat. Int. 29, 119-
736 128.

737 Walther, J., 1894, Einleitung in die Geologie als historische Wissenschaft. In Lithogenesis
738 der Gegenwart. Jena: G. Fischer, Bd. 3, pp. 535-1055.

739 Wanner, H., Solomina, O., Grosjean, M., Ritz, S.P., Jetel, M., 2011. Structure and origin of
740 Holocene cold events. Quaternary Science Reviews 30, 3109-3123.

741 Zazo, C. (2006). Cambio climático y nivel del mar: la Península Ibérica en el contexto
742 global. Rev. Cuat. y Geom., 20, 115-130.

743

744 FIGURE CAPTIONS AND TABLES

745 Figure 1. (a) Geographical and geological setting and location of cores. Detail of Almenara
746 (b) and (c) Benicasim mashes and position of the cores with geochemical data. Orthophotos
747 provided by the Spanish Geographical Institute (IGN).

748

749 Figure 2. Stratigraphic sections for cores recovered at Almenara-Nules and Benicasim
750 marshes with indication of facies, environments and sequences/cycles (modified from
751 Mediato, 2016).

752

753 Figure 3. Biplot of the two main principal components for the raw geochemical dataset and
754 the Al-normalized values.

755

756 Figure 4. Facies and geochemical record for the cored of Almenara and Benicasim marshes
757 for cycles 1 and 2. Facies and trend key as for figure 2. Radiocarbon samples (from the
758 whole set of cores in Fig. 2) arrangement relative to sequence boundaries. Grey stripes: Ca,
759 Mg/Al, S/Al, Na/Al and Mn/Fe increases.

760

761 Figure 5. Conceptual model of the deepening-shallowing cycle. a) Deepening sequence
762 resulting from sea level (base level) rise not balanced by sedimentation (A>S). b)
763 Shallowing sequence as result of sedimentation rate greater than rate of sea level rise (A<S),
764 c) Cycle development as consequence of changes in the rate of relative sea level rise.

765

766 Figure 6. Correlation of sedimentary cycles for the Almenara marsh and sea level changes
767 at different locations of the Spanish Mediterranean coast.

768

769 Figure 7. Conceptual model for the sea level and climate relation to geochemical
770 composition. Big arrows point to the displacement of the water levels. The depicted
771 elements increase for the conditions depicted in each sketch. Upper row: rising sea level;
772 middle row: stable sea level; lower row: falling sea level. Left column: wet periods; right
773 column: arid periods. Thick line: boundary of marine-terrestrial groundwater (MTGB);
774 white arrow: sense of displacement of the MTGB.

775

776 Figure 8. Comparison of salinity periods to environmental evolution of nearby coastal
777 lagoons, aridity records in marine and terrestrial Spanish areas, lake levels in central Europe
778 and fluvial activity in Spain.

779

780 Figure 9. Salinity/aridity episodes and their comparison to global dry periods,
781 paleoceanographic (SST), atmospheric (NAO index) and solar (Total Solar Irradiance and
782 sunspot numbers).

783

784 Table 1. Radiocarbon samples and dates for the studied cores.

Core	Lab Sample number	Depth (cm)	^{14}C age (BP)	Method	δ^{13}C	Lithology	Calibrated ^{14}C age (2σ)
C 3	GdA-657	21	715 ± 35	AMS	-10,8 ± 0,4	Silt	[644-724 BP]
C 3	GdA-658	51	820 ± 35	AMS	-22,6 ± 0,7	Silt	[679-789 BP]
C 3	Gd-30095	157	4870 ± 100	Radiocarbon standard	-25	Peat	[5445-5766 BP]
C 6	GdA-649	79	610 ± 35	AMS	-31,5 ± 0,6	Peat	[544-656 BP]
C 6	GdA-648	265	3690 ± 35	AMS	25,6 ± 0,5		[3922-4098 BP]
C 7	GdA-650	130	Modern 114,96 ± 0,41 pMC	AMS	-25,9 ± 0,2	Organic-rich sediment	-----
C 7	Gd-30096	344	5020 ± 120	Radiocarbon standard	-25	Peat	[5576-6003 BP]
C 8	GdA-651	69	Modern 124,43 ± 0,46 pMC	AMS	-28,6 ± 0,3	Organic-rich sediment	-----
C 8	Gd-17366	172	3800 ± 140	Radiocarbon standard	-25	Peat	[3826-4574 BP]
C 10	GdA-616	48	Modern 109,68±0,37 pMC	AMS	-30,7 ± 0,6	Organic-rich sediment	-----
C 10	GdA-501	140	270 ± 40	AMS	-28,8 ± 0,4	Peat	[346-464 BP]
C 10	Gd-30094	191	3320 ± 95	Radiocarbon standard	-25	Peat	[3366-3732 BP]
Benicasim	GdA-500	360	5150 ± 40	AMS	-26,3 ± 0,9	Peat	[5875-5991 BP]
Nules	GdA-503	485	5920 ± 70	AMS	-29,3 ± 0,3	Peat	[6601-6936 BP]

785

786 Table 2. Eigenvectors for the two main principal components for the raw geochemical
787 dataset and the Al-normalized values. Bold-italics: main positive values; bold: main
788 negative values.

Raw dataset							Al-normalized values						
	C7		C3		C10			C7		C3		C10	
	PC1	PC2	PC1	PC2	PC1	PC2		PC1	PC2	PC1	PC2	PC1	PC2
Al	**-0.303**	0.059	**-0.290**	0.074	***0.295***	-0.164							
Si	**-0.296**	0.091	**-0.291**	0.043	***0.308***	0.094	Si/Al	-0.040	**-0.547**	***0.184***	***0.363***	***0.292***	***0.330***
Fe	**-0.219**	-0.096	**-0.274**	-0.035	***0.290***	-0.027	Fe/Al	***0.241***	-0.094	***0.231***	-0.095	-0.123	***0.445***
Ca	***0.246***	***0.258***	***0.290***	-0.051	**-0.247**	***0.288***	Ca/Al	***0.281***	-0.040	***0.251***	-0.002	**-0.277**	***0.215***
Mg	**-0.297**	0.088	**-0.283**	***0.105***	0.135	-0.021	Mg/Al	***0.281***	-0.061	***0.248***	0.034	**-0.276**	***0.215***
Na	**-0.270**	0.002	**-0.240**	***0.346***	-0.150	**-0.440**	Na/Al	-0.011	***0.483***	***0.216***	***0.318***	**-0.277**	**-0.240**
K	**-0.291**	0.082	**-0.291**	-0.023	***0.315***	0.024	K/Al	**-0.222**	-0.156	**-0.170**	***-0.491***	***0.314***	***0.210***
Cr	-0.153	0.024	-0.017	-0.058	0.183	0.007	Cr/Al	0.034	0.167	***0.178***	-0.216	0.125	***0.160***
Ti	**-0.300**	0.061	**-0.291**	0.023	***0.313***	-0.003	Ti/Al	**-0.168**	**-0.459**	**-0.182**	***-0.500***	***0.276***	***0.345***
Mn	0.122	***0.303***	0.065	***0.590***	***0.226***	***0.260***	Mn/Al	***0.229***	0.086	***0.223***	-0.149	-0.157	***0.540***
P	-0.078	0.167	**-0.268**	-0.133	***0.219***	**-0.342**	P/Al	***0.251***	0.171	***0.246***	-0.065	-0.183	0.058
Sr	***0.250***	***0.206***	***0.254***	***0.303***	**-0.300**	-0.058	Sr/Al	***0.282***	0.006	***0.247***	-0.025	**-0.328**	***0.113***
Ba	**-0.257**	0.127	**-0.241**	0.223	***0.219***	**-0.301**	Ba/Al	***0.255***	-0.105	***0.250***	-0.024	**-0.208**	***0.203***
B	**-0.242**	0.087	**-0.282**	-0.076	0.104	**-0.437**	B/Al	-0.086	***0.340***	***0.201***	***-0.376***	**-0.224**	-0.025
S	-0.059	**-0.331**	-0.063	**-0.584**	**-0.263**	**-0.296**	S/Al	***0.253***	-0.135	***0.251***	-0.138	**-0.327**	-0.051
C_{in}	***0.205***	***0.309***					C_{in}/Al	***0.273***	-0.052				
C_{org}	0.058	**-0.414**					C_{org}/Al	***0.261***	-0.036				

789

Declaration of interests

☒ The authors declare that they have no known competing financial interests or personal relationships that could have appeared to influence the work reported in this paper.

☐The authors declare the following financial interests/personal relationships which may be considered as potential competing interests: